

# Ligand-Field Energy Splitting in Lanthanide-Based Single-Molecule Magnets by NMR Spectroscopy

Markus Hiller,<sup>†</sup> Saskia Krieg,<sup>†</sup> Naoto Ishikawa,<sup>‡,b</sup> and Markus Enders<sup>\*,†,b</sup>

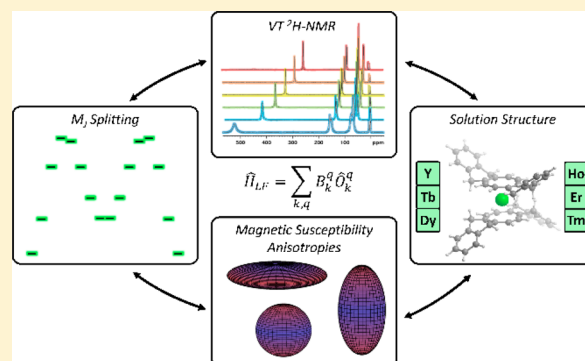
<sup>†</sup>Institute of Inorganic Chemistry, Heidelberg University, Im Neuenheimer Feld 270, 69120 Heidelberg, Germany

<sup>‡</sup>Department of Chemistry, Graduate School of Science, Osaka University, Toyonaka, Osaka 560-0043, Japan

**S** Supporting Information

**ABSTRACT:** A method for the experimental determination of ligand-field (LF) energy splitting in mononuclear lanthanide complexes, based purely on variable-temperature NMR spectroscopy, was developed. The application of this method in an isostructural series of anionic lanthanide bis(cyclooctatetraenide) double-decker compounds bearing large rigid substituents is demonstrated. Using the three-nuclei plot approach devised by Reilley, the isostructurality of the compound series and the identical orientation of the magnetic main axis of all Ln<sup>3+</sup> ions in the series Tb<sup>3+</sup> to Tm<sup>3+</sup> are demonstrated. Measurement of the <sup>2</sup>H NMR spectra of partially deuterated analogues of the complexes permitted determination of the axial magnetic susceptibility anisotropies  $\chi_{ax}$  for all five ions in the temperature range from 185 to 335 K. For this purpose, analysis of the hyperfine shifts was combined with structural models derived from density functional theory calculations.

In a final step, the temperature dependence of the  $\chi_{ax}$  values was used for determination of the three axial LF parameters, adapting a method employed previously for phthalocyanine-based systems. The temperature dependence dictated by the LF parameters determined by this NMR-based approach is compared to the results of recently published ab initio calculations of the system, indicating reasonable agreement of both methods. For all ions except Dy<sup>3+</sup>, the NMR method determines the same  $m_j$  ground state as the calculations and the order and energies of the excited states match well. However, the sign of the magnetic anisotropy of the dysprosium complex in the temperature range evaluated here is not correctly predicted by the published calculations but can be described accurately by the NMR approach. This shows that our experimental method for determination of the LF parameters is an ideal complementation to other theoretical and experimental methods.



## INTRODUCTION

The rational design of coordination compounds with single or a few lanthanide centers has led to a dramatic increase of the anisotropy barriers of single-molecule magnets (SMMs).<sup>1–8</sup> The current record in the blocking temperature is 60 K in an axially coordinated dysprosium compound.<sup>2,3</sup> The main point of control for a further increase of the magnetic anisotropy barrier in SMMs with single lanthanide centers is the ligand field (LF), which causes energy splitting of the  $2J + 1$  levels in the spin–orbit-coupled  $J$  ground state. The LF can be described quantitatively by the LF parameters, and their theoretical and experimental determination is a prerequisite for a thorough understanding of the relationship between the ligand environment and SMM behavior.<sup>9</sup> Consequently, methods for a fast and reliable determination of the LF parameters are very important for SMM research.<sup>10,11</sup> Usually, this is achieved by an investigation of luminescence<sup>12–14</sup> or torque magnetometry measurements.<sup>15</sup> However, up to 27 LF parameters may contribute to the energy splitting, and therefore their experimental determination is often hampered by over-parametrization. The situation is simplified if the ligand environment leads to a higher symmetry, which is the case

for many axial SMMs. Ishikawa et al. combined paramagnetic NMR shifts and SQUID magnetization data in order to obtain LF parameters in phthalocyaninide (Pc)-based double- and triple-decker compounds.<sup>16,17</sup> This allowed for the prediction and validation of the SMM behavior for Pc<sub>2</sub>Tb, which had the highest anisotropy barrier to date<sup>18</sup> and is one of the most studied SMM systems. In the last years, NMR has been applied in a growing number of studies for the investigation of SMMs and related compounds.<sup>19–26</sup> In this work, a purely NMR-based method for determination of the LF parameters in cyclooctatetraenide-based lanthanide double-decker complexes is described. This class of SMMs was first introduced by Long, Murugesu, and co-workers.<sup>27–30</sup> The methodology presented here is based on the fact that each of the  $2J + 1$  substates is connected to a magnetic anisotropy. The energetic splitting of this  $m_j$  manifold by the LF leads to an overall, temperature-dependent anisotropy of the magnetic susceptibility. This resulting axial anisotropy  $\chi_{ax}$  can be determined quickly and reliably by NMR measurements. The advantage of a solution

Received: October 24, 2017

method for LF parameter determination is the fact that the magnetic molecules are well separated from each other and hence intermolecular interactions do not hamper analysis. Simultaneously, recent results show that the treatment of the structure in solution requires careful consideration.<sup>31</sup>

Depending on the ligand environment, different lanthanide ions lead to easy-plane or easy-axis magnetization. The latter is a prerequisite of the SMM behavior. Cyclic polydentate ligands like derivatives of Pc or COT have been utilized extensively for the synthesis of double-decker-type SMMs. In the case of monoanionic compounds of the type  $[\text{Ln}(\text{COT}')_2]^-$  ( $\text{COT}' =$  substituted cyclooctatetraenide), the  $\text{Er}^{3+}$  and  $\text{Dy}^{3+}$  compounds exhibit slow relaxation of magnetization.<sup>28–30</sup> In a recent study, we demonstrated the application of two new ligand derivatives, easily accessible by dimerization of dialkynes.<sup>25,32</sup> The axial magnetic susceptibility anisotropies ( $\chi_{\text{ax}}$ ) of the lanthanide complexes from  $\text{Tb}^{3+}$  to  $\text{Tm}^{3+}$  could be determined by a simultaneous analysis of the NMR spectra of the series. The analysis revealed, that, for the  $\text{Dy}^{3+}$ ,  $\text{Er}^{3+}$ , and  $\text{Tm}^{3+}$  ions,  $\chi_{\text{ax}}$  is positive; i.e., the magnetization along the magnetic main axis is larger than that in the perpendicular direction, which is a requirement for SMMs. While this observation is in agreement with the observed magnetic behavior, it is in striking contrast to the classic Bleaney approach, which predicts a different sign of  $\chi_{\text{ax}}$  for  $\text{Dy}^{3+}$  and  $\text{Tm}^{3+}$ .<sup>33</sup> Several recent reports indicate that the assumptions used by Bleaney, particularly the comparable population of all  $m_j$  levels, are not satisfied in compounds with large magnetic anisotropies typical for SMMs and related systems.<sup>34,35</sup>

The classification of the lanthanide ions as prolate ( $\text{Er}^{3+}$ ,  $\text{Tm}^{3+}$ , and  $\text{Yb}^{3+}$ ) and oblate ( $\text{Tb}^{3+}$ ,  $\text{Dy}^{3+}$  and  $\text{Ho}^{3+}$ ) groups, depending on the asphericity of their respective ground states, has been suggested as a guideline for the choice of a suitable ligand environment.<sup>1,36</sup> Within this framework, oblate ions should be combined with axial LFs in order to enhance the SMM properties, whereas for prolate ions, equatorial LFs should be applied. The recently reported dysprosocenium system<sup>2,3</sup> exploits this approach with impressive results. However, this simple and useful tool must be applied with care because the ground state, and thus the classification as oblate/prolate, is subject to the influence of the LF. This is demonstrated by the  $\text{Dy}(\text{COT})_2^-$  system because it represents the combination of a typical oblate ion and an equatorial LF. This peculiarity can be explained by computational investigations of the system,<sup>37,38</sup> which showed that the lowest-lying  $m_j$  substate is the  $|\pm^9/2\rangle$  doublet, exhibiting a slightly prolate shape.

For closer insight into the electronic structure of the ions from experimental data, it is necessary to determine the temperature dependence of the  $\chi_{\text{ax}}$  values. In this work, the ligand (6Z,14Z)-5,8,13,16-tetrahydrocycloocta[1,2-b:5,6-b']-dinaphthalene (tdnCOT) was prepared<sup>32,39</sup> and used for the synthesis of new lanthanide double-decker complexes. tdnCOT offers the advantage of increased distance between the NMR-active nuclei and paramagnetic ion. Consequently, the line widths of the NMR signals of the double-decker complexes are smaller, allowing signal detection at lower temperatures. Additionally, the straightforward introduction of  $^2\text{H}$  nuclei is possible, further decreasing the signal line widths due to the smaller gyromagnetic ratio.<sup>40,41</sup> Finally, the quadrupole moment of  $^2\text{H}$  introduces the opportunity for the detection of residual quadrupolar couplings (RQCs) due to partial align-

ment in solution, which can be used to determine the magnetic susceptibility anisotropies by an independent approach.<sup>42</sup>

## RESULTS

A new series of lanthanide cyclooctatetraenide sandwich complexes was synthesized by the reduction of tdnCOT and subsequent reaction with anhydrous lanthanide trichlorides (Scheme 1). This method was previously employed for similar

### Scheme 1. Synthesis of the $\text{Li}(\text{MeCN})[\text{Ln}(\text{tdnCOT})_2]$ Complex Series<sup>a</sup>



<sup>a</sup>The substituents are drawn schematically without regard for their conformation. The blue numbers indicate the NMR signal assignment.

systems.<sup>25</sup> The five trivalent lanthanide ions from  $\text{Tb}^{3+}$  to  $\text{Tm}^{3+}$  were investigated because these are characterized by large magnetic moments and anisotropies. The corresponding  $\text{Y}^{3+}$  compound was chosen as a diamagnetic reference. The complexes were obtained in yields ranging from 40 to 67% as orange ( $\text{Tb}^{3+}$ ), brown ( $\text{Tm}^{3+}$ ) or yellow ( $\text{Y}^{3+}$ ,  $\text{Dy}^{3+}$ ,  $\text{Ho}^{3+}$ , and  $\text{Er}^{3+}$ ) powders and contained acetonitrile (MeCN), as determined by elemental analysis and NMR spectroscopy. The compounds are readily soluble in tetrahydrofuran (THF) and, to a smaller extent, in MeCN. Because of their ionic nature, the solubility in noncoordinating solvents including dichloromethane is severely limited, despite the large substituents.

**NMR Spectroscopy.** The NMR measurements were carried out with THF as the solvent because it allows measurement at lower temperatures in comparison to MeCN. The  $^1\text{H}$  and  $^{13}\text{C}$  NMR spectra at room temperature (Figure 1) consist of a maximum of five and six signals, respectively. This agrees well with the expected high molecular symmetry ( $D_2$  or  $S_4$ ). Assignment of the signals was achieved primarily on the basis of their respective line widths, as described in detail in the Supporting Information (SI).

Analysis of the NMR spectra was achieved according to a methodology based on the three-nuclei plot introduced by Reilly,<sup>43,44</sup> which was used previously for the  $\text{Li}[\text{Ln}(\text{odbCOT})_2]$  and  $\text{Li}[\text{Ln}(\text{hdcCOT})_2]$  series.<sup>25</sup> This method assumes approximately identical structures for the entire series of investigated compounds and was successfully applied in a variety of systems.<sup>43,45,46</sup> Two important consequences result from this approximation. First, the propagation of the spin density through the ligand can be assumed to be identical for all compounds; i.e., the hyperfine coupling constant  $A^i/\hbar$  of a particular nucleus  $i$  is independent of the investigated lanthanide ion  $j$  and identical throughout the series. The second important simplification of this approach is that the geometric factor  $G^i$  of the investigated nucleus is independent of the investigated lanthanide ion as well and constant within the series.  $G^i$  depends on the metal–nucleus distance  $r^i$  as well as the polar angle  $\theta^i$  with respect to the main magnetic axis. The latter is assumed to be identical for all lanthanide ions,<sup>43,44</sup> which is plausible for highly symmetric coordination environments such as in the system investigated here but not necessarily in lower symmetry.<sup>26,47</sup> Under the condition of isostructurality, the hyperfine shifts of all nuclei in all complexes

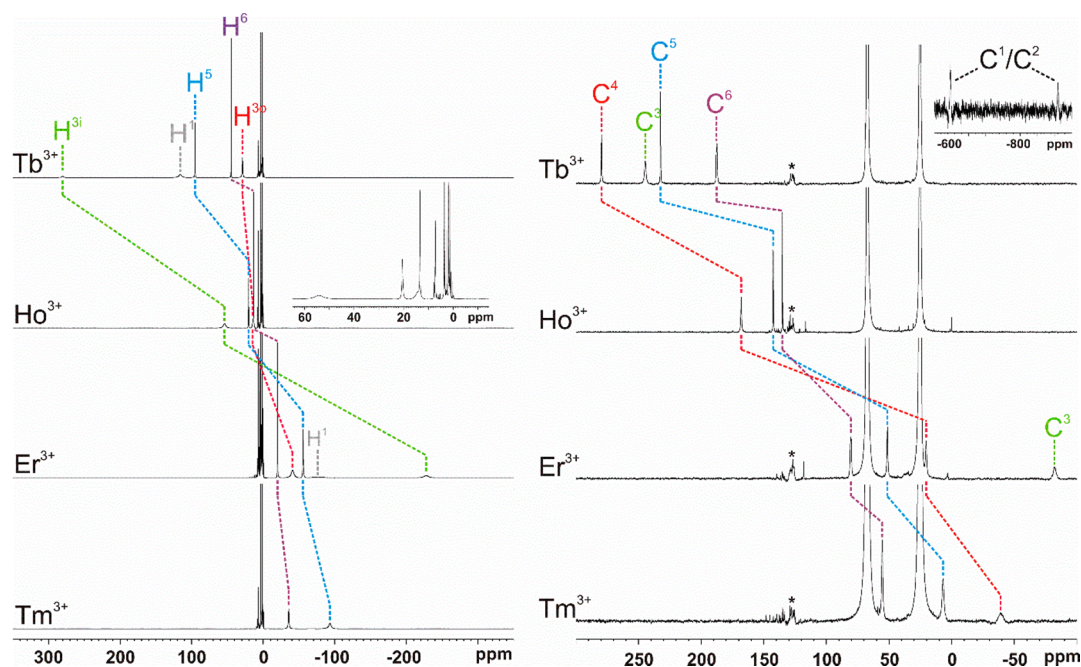


**Figure 1.**  $^1\text{H}$  (left) and  $^{13}\text{C}\{^1\text{H}\}$  (right) NMR spectra (14.1 T, 295 K,  $\text{THF-}d_8$ ) of the individual ions in the  $\text{Ln}(\text{tdnCOT})_2^-$  series. The ions are ordered with increasing  $\chi_{\text{ax}}$  values, resulting in monotonic shifts of the individual signals along the series. The  $\text{Dy}^{3+}$  ion is omitted for clarity because it exhibits very small shifts. Signals marked with asterisks refer to decomposition products.

of a series can be expressed by eq 1 if only axial anisotropy of the magnetic susceptibility  $\chi_{\text{ax}}^j$  is present.

$$\delta_{\text{HF}}^{i,j} = \frac{\mu_{\text{B}}}{3kT\gamma^i} \frac{A^i}{\hbar} \langle S_z \rangle^j + \frac{1}{12\pi} G^i \chi_{\text{ax}}^j \quad (1)$$

In eq 1, the first product corresponds to the Fermi contact term, with  $\mu_{\text{B}}$  representing the Bohr magneton,  $k$  the Boltzmann constant,  $T$  the absolute temperature, and  $\gamma^i$  the gyromagnetic ratio of the nucleus under consideration. The quantity  $\langle S_z \rangle^j$  is the average reduced spin polarization, which was taken from the literature.<sup>43–46</sup> The second product is the pseudocontact shift.

The approximations discussed above are easily verified by a so-called three-nuclei plot by plotting a property  $Y^i$  (Figure 2) calculated from the observed hyperfine shifts and the literature values of  $\langle S_z \rangle^j$ . The data points for the individual nuclei positions show a linear dependence, which confirms both the assignment of the signals and the validity of the three-nuclei approach for this complex series. In addition, it is demonstrated clearly that the main magnetic axes are identical for all lanthanide ions and that no relevant rhombic components of the magnetic susceptibility anisotropy are present. The slopes of the linear functions indicated in Figure 2 correspond to the ratio of the geometric factors of the individual nuclei with respect to the  $\text{H}^{3i}$  position (cf. Figure 3) serving as a reference.

If no structural information (i.e., geometric factors  $G^i$ ) is available, the NMR spectra can be investigated using relative geometric factors and susceptibility anisotropies, as demonstrated successfully in a previous study.<sup>25</sup> Because the values of both  $G^i$  and  $\chi_{\text{ax}}^j$  in eq 1 are unknown in this case, the geometric factor is fixed to unity for one arbitrarily chosen nucleus (here  $\text{H}^{3i}$ ; see Figure 3). Through fitting of the observed hyperfine shifts, the relative geometric factors  $G^i = G^i/G^{\text{ref}}$  are obtained for the remaining nuclei. The ratio of the geometrical and relative geometric factors is identical for any two nuclei. This

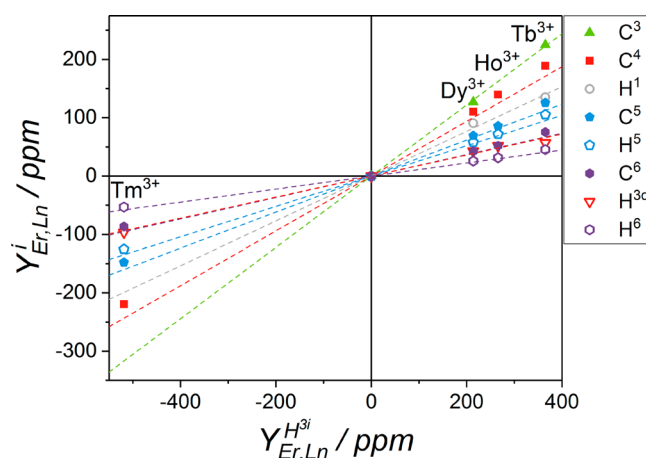


**Figure 2.** Three-nuclei plot of all detectable signals in the  $\text{Ln}(\text{tdnCOT})_2^-$  series at 295 K. The  $\text{Er}^{3+}$  ion and the  $\text{H}^{3i}$  position were chosen as references. Consequently, the data points representing the  $\text{H}^{3i}$  position are arranged horizontally, while the values for the remaining nuclei are displayed in the vertical direction. The values  $Y$  are calculated as  $Y_{\text{Er,Ln}}^i = \delta_{\text{HF,Ln}}^i \langle S_z \rangle_{\text{Er}} / \langle S_z \rangle_{\text{Ln}} - \delta_{\text{HF,Er}}^i$ . Lines represent the best linear fits through the origin.

method is described in more detail in the SI and is particularly beneficial if the solution-averaged structure cannot be represented by a single structure due to flexibility, as in the present case.

Because of the relatively rigid substituents, only one dynamic process appears likely, corresponding to the interchange of the two possible arrangements of the cyclohexadiene motifs ( $\text{C}^2$ ,  $\text{C}^3$ , and  $\text{C}^4$  positions). This “flapping” of the benzene moieties can be represented by two molecular conformations, where all four substituents point inward (all-endo conformation) or outward (all-exo conformation). Naturally, three further combinations are possible. However, the above extreme cases

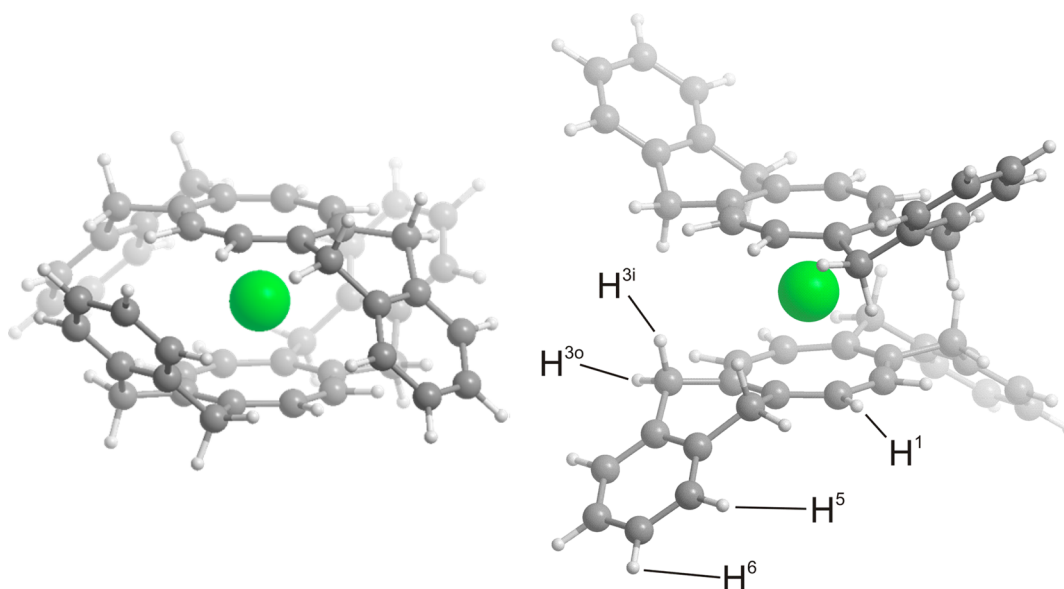


**Figure 3.** DFT-optimized structures (B3LYP, Def2TZVP/6-311g, and GD3) of  $Y(\text{tdnCOT})_2^-$  in the all-endo (left) and all-exo (right) conformations. The labeling of the  $^1\text{H}$  nuclei, as was used for the NMR assignment, is included.

are the limitations for the geometric factors, and thus these two possibilities were explored by density functional theory (DFT) optimization (B3LYP and Def2TZVP/6-311g), the results of which are displayed in Figure 3. Depending on the method used, either the all-exo (calculations without dispersion correction) or the all-endo (calculations with dispersion correction) conformer is slightly favored energetically. This result is in accordance with the NMR data, which show that each of the four benzene groups can adopt an endo or exo orientation in solution (see below).

A comparison of the relative geometric factors (listed in Table S9) obtained from the fitting of the hyperfine shifts to eq 1 shows that neither the all-endo nor the all-exo conformation gives good agreement. However, if a ratio of all-endo/all-exo of approximately 1:1 is assumed, excellent agreement is observed (Figure 4). This suggests that at ambient temperature, on average, two of the four benzene cores point inward and outward, respectively, and that the reorientation is fast on the NMR time scale. Note that, for calculation of the relative geometric factors, the vector connecting the  $\text{C}_8$  centroids was presumed to represent the magnetic main axis. The excellent agreement depicted in Figure 4 and the three-nuclei plot in Figure 2 demonstrate clearly that, in the  $\text{Ln}(\text{tdnCOT})_2^-$  system, this assumption is justified. However, in systems with lower symmetry, the magnetic axis system does not necessarily coincide with molecular symmetry elements. Analysis of the temperature dependence of the  $^2\text{H}$  NMR spectra shows that the relative geometric factors derived from the three-nuclei plots change approximately linearly with the temperature (see Figure S17). This behavior was successfully described by a temperature-dependent ratio of the two conformers (Table S15). On the basis of the determined mixture of both conformations at the different temperatures and the geometric factors calculated from the model geometries, the relative geometric factors of all nuclei were calculated. With these relative geometric factors describing the solution average, the magnetic susceptibility anisotropies summarized in Table 1 were obtained.

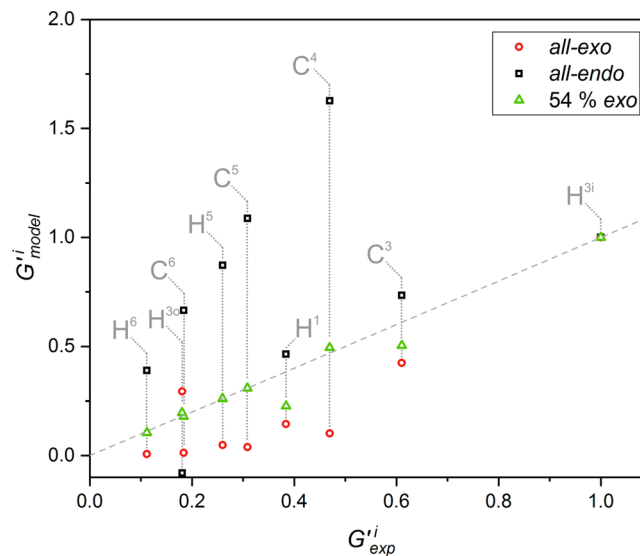


**Figure 4.** Comparison of the experimentally derived relative geometric factors (horizontal) with the values obtained from the DFT-optimized structures (black and red) and the solution average (green). The gray line represents perfect agreement. Note that the position of the  $\text{H}^1$  (COT-H) nucleus is poorly represented in all three models.

**Table 1. Magnetic Susceptibility Anisotropies at 295 K Obtained by the Fitting Procedure and from the RQC Splitting<sup>a</sup>**

$\text{Ln}^{3+}$	$\chi_{\text{ax}} (\times 10^{-31} \text{ m}^3)$	
	fit	RQC
$\text{Tb}^{3+}$	$-8.30 \pm 2.03$	$-8.58 \pm 0.37$
$\text{Dy}^{3+}$	$0.711 \pm 0.098$	$1.00 \pm 0.09$
$\text{Ho}^{3+}$	$-1.58 \pm 0.27$	$-1.30 \pm 0.10$
$\text{Er}^{3+}$	$6.48 \pm 0.91$	$6.56 \pm 0.30$
$\text{Tm}^{3+}$	$10.48 \pm 1.19$	$10.46 \pm 0.44$

<sup>a</sup>The signs of the latter were chosen in order to agree with the first set. The given uncertainties for the values from the fit are standard deviations due to the use of geometric factors of different positions.

The possibility of introducing  $^2\text{H}$  nuclei in a straightforward manner permits detection of the corresponding  $^2\text{H}$  NMR signals within the entire liquidity range of the solvent (THF), thus allowing determination of the susceptibility anisotropies at significantly lower temperatures than was possible for the previously investigated series.<sup>25</sup> Additionally, the quadrupole moment of  $^2\text{H}$  gives a second, independent approach for determination of the  $\chi_{\text{ax}}^j$  values. The large magnetic anisotropies of the molecules lead to a partial alignment in the magnetic field of the NMR spectrometer; i.e., they orient partially in such a way that the largest susceptibility tensor component is aligned with the magnetic field direction. As a result, the signals of nuclei with  $I > 1/2$  may show RQC and are split into  $2I$  lines, which may, however, be obscured by the line widths of the signals. The size of the observable RQC can be described by eq 2,<sup>47,48</sup> wherein  $B_0$  represents the magnetic flux density,  $\mu_0$  the vacuum permeability, and  $e^2qQ/h$  the nuclear quadrupole coupling constant. A value of 186 kHz for the C–D quadrupolar coupling constant has been used in this work for the aromatic  $\text{D}^5$  position;<sup>49</sup> for the methylene group, no precise literature value is available. Presumably, the value is between those reported for  $\text{CD}_2\text{Cl}_2$  (160 kHz) and cyclohexane- $d_{12}$  (174 kHz).<sup>50</sup> Furthermore, RQCs are dependent on the angle  $\alpha$ , which is measured between the main magnetic axis and electric field gradient surrounding the quadrupolar nucleus, which is defined by the C–D bond vector. Because of the connectivity of the employed ligand, in both conformers (all-endo and all-exo), the main magnetic axis of the compounds (assumed to coincide with the vector connecting the  $\text{C}_8$  centroids) and the  $\text{C}^5$ – $\text{D}^5$  bond are perpendicular, resulting in an angle  $\alpha$  of  $90^\circ$ . Consequently, the RQC splitting of  $\text{D}^5$  is independent of the flexibility of this molecule and ideal for an additional determination of  $\chi_{\text{ax}}$ . In eq 2,  $\chi_{\text{ax}}$  represents the anisotropy of the entire molecule, including contributions from the diamagnetic ligands. However, the latter lies in the range of 0.5 Hz for deuterobenzene (same magnetic field as that used in this study)<sup>51</sup> and is therefore negligible compared to the anisotropy resulting from the lanthanide center. It should be noted that the sign of the anisotropy cannot be determined directly from the splitting.

$$|\Delta\nu_{\text{Q}}| = \left| \frac{(e^2qQ/h)B_0^2}{20\mu_0kT} (3 \cos^2 \alpha - 1) \chi_{\text{ax}} \right| \quad (2)$$

The effects of the RQC splitting can be observed best in the  $^2\text{H}$  NMR spectrum of the  $\text{Tb}^{3+}$  analogue, displayed in Figure 5. As expected, the splitting is largest for  $\text{D}^5$  (310 Hz). Additionally, splittings are observed for the  $\text{D}^{30}$  (116 Hz) and  $\text{D}^{3i}$  resonances (not fully resolved). For the remaining ions,

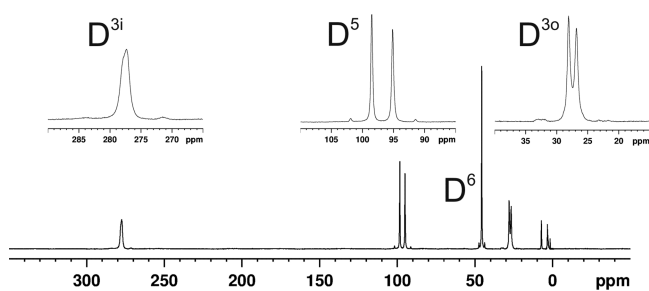


**Figure 5.**  $^2\text{H}$  NMR spectrum (14.1 T, 295 K, THF) of  $\text{Tb}(\text{tdnCOT})_2^-$ .

larger line widths are observed, leading to an observable splitting only for the respective signals of  $\text{D}^5$ . Notably, the narrowest signal ( $\text{D}^6$ ) reveals no splitting in any of the complexes, indicating that the orientation of the corresponding C–D bond leads to an angle close to  $54^\circ$ , minimizing the absolute value of the  $3 \cos^2 \alpha - 1$  expression (eq 2). From the size of the splitting of  $\text{D}^5$ , observable for all ions at 14.1 T (295 K), a second set of  $\chi_{\text{ax}}$  values was obtained (see Table 1). For this purpose, an angle  $\alpha$  of  $90 \pm 3^\circ$  was used for the calculation with eq 2, in agreement with the DFT-optimized structures of both conformations. The angles for the remaining positions depend on the conformation and are summarized in Table S12. The magnetic anisotropy values obtained from analysis of the hyperfine shifts (eq 1) and from the RQC data agree well.

The temperature dependence of the  $^2\text{H}$  NMR signals could be measured over the entire liquidity range of the solvent THF and is represented for the  $\text{Tb}^{3+}$  ion in Figure 6. Using the

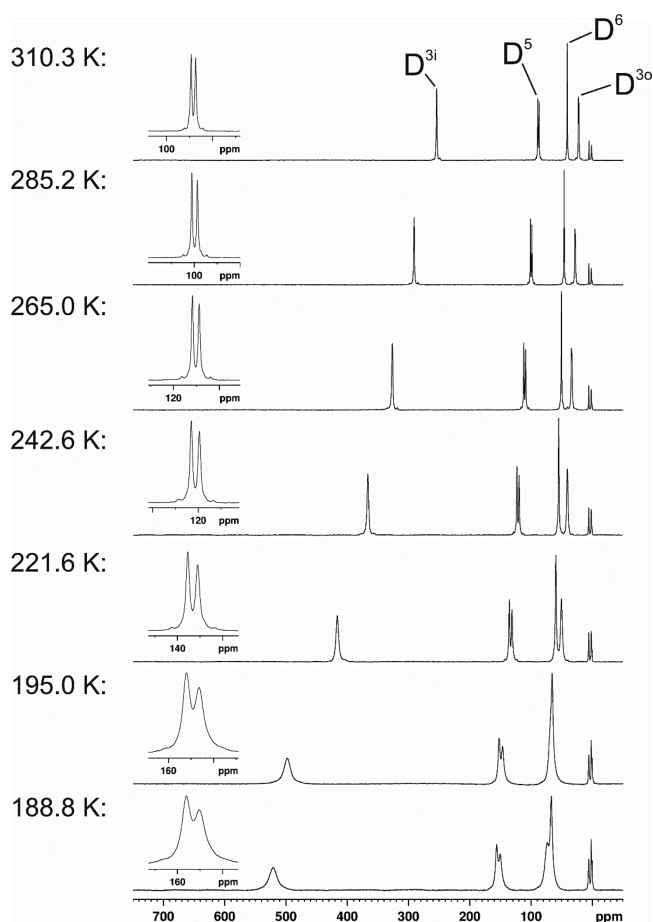


**Figure 6.** Variable-temperature  $^2\text{H}$  NMR spectra (61.4 MHz, THF) of  $\text{Tb}(\text{tdnCOT})_2^-$  with expansion of the  $\text{D}^5$  signal, showing the RQC splitting.

chemical shifts of four nuclei positions ( $\text{D}^{3i}$ ,  $\text{D}^{30}$ ,  $\text{D}^5$ , and  $\text{D}^6$ , identical with the designation in Figure 3) in the complexes of the five ions  $\text{Tb}^{3+}$ – $\text{Tm}^{3+}$  at eight different temperatures permitted determination of the temperature dependence of the magnetic susceptibility anisotropies  $\chi_{\text{ax}}^j$ , as depicted in Figure 7. Details of the procedure are provided in the SI.

Figure 7 shows the variation of the susceptibility anisotropies with temperature, which strongly depends on the lanthanide ion. For  $\text{Tb}^{3+}$  and  $\text{Ho}^{3+}$  in the entire temperature range easy-

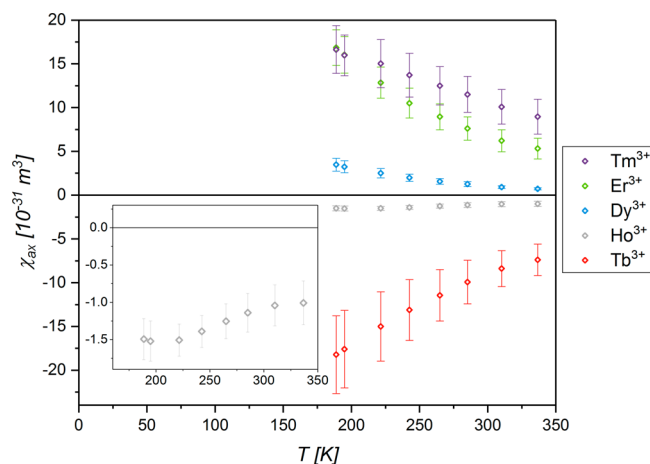


**Figure 7.** Temperature dependence of the magnetic susceptibility anisotropies for the individual ions in  $\text{Ln}(\text{tdnCOT})_2^-$ . The values for the  $\text{Ho}^{3+}$  analogues are enlarged in the inset.

plane anisotropy is observed, while the remaining ions are easy-axis systems. However, the  $\text{Tb}^{3+}$ ,  $\text{Dy}^{3+}$ , and  $\text{Er}^{3+}$  ions show variations that resemble hyperbolas, while the  $\text{Tm}^{3+}$  ion follows a rather linear dependence. Finally, the curve of the  $\text{Ho}^{3+}$  ion is consistent with the presence of an inflection point, and upon further lowering of the temperature, the anisotropy is indicated to decrease, which is, at first glance, a rather unexpected behavior. However, it can be explained by the  $m_j$  level splitting described below. The small value of  $\chi_{\text{ax}}$  for the  $\text{Dy}^{3+}$  ion is rather unexpected considering the reported SMM behavior of such systems.<sup>27,28,52</sup> However, computational analyses<sup>37</sup> determined the lowest Kramers doublet to be composed mainly of the  $m_j = |\pm 9/2\rangle$  states, which possess smaller intrinsic anisotropies compared to the Ising ground states  $m_j = |\pm 15/2\rangle$  and  $m_j = |6\rangle$  for the  $\text{Er}^{3+}$  and  $\text{Tm}^{3+}$  ions, respectively. The LF parameters determined here confirm these results; however, the  $m_j = |\pm 11/2\rangle$  state is determined as the ground state for  $\text{Dy}^{3+}$  (see below).

**SQUID Magnetic Measurements.** For a powdered sample of the  $\text{Er}^{3+}$  compound, a magnetic hysteresis loop could be measured at 2 K, which is closed at zero field. This behavior and the saturation magnetization are similar to those of related systems.<sup>29,30</sup> For neither the  $\text{Dy}^{3+}$  nor  $\text{Tm}^{3+}$  complex, hysteresis was observed under identical measurement conditions (Figure 8). This is in agreement with data for a related  $\text{Dy}^{3+}$  derivative.<sup>28</sup> Very recent results of Murugesu et al. confirm the SMM behavior of the  $\text{Tm}^{3+}$  ion in the  $\text{COT}_2$  environment.<sup>53</sup>

**Determination of the LF Parameters.** The  $\text{Ln}(\text{COT})_2^-$  sandwich system represents a particularly suitable system for determination of the LF parameters if a  $D_{8h}$ -symmetric environment of the lanthanide ions is assumed. In this case, the LF Hamiltonian acting on the  $2J + 1$   $m_j$  states of the  $J$  manifold of the lanthanide ion only contains three axial terms, as described by eq 3. The associated spin operator matrices only possess nonzero elements along the diagonal. Thus, the wave functions correspond to the pure  $m_j$  states of the free ions; i.e., there is no mixing of these states.

$$\hat{H}_{\text{LF}} = B_2^0 \hat{O}_2^0 + B_4^0 \hat{O}_4^0 + B_6^0 \hat{O}_6^0 \quad (3)$$

The matrix elements of the spin equivalent operators  $\hat{O}_k^q$  (eq 3) are tabulated in the literature.<sup>54</sup> The associated values  $B_k^q$  are

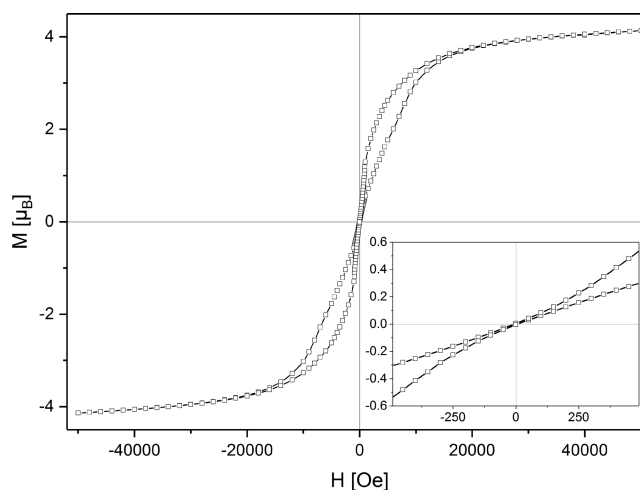


**Figure 8.** Hysteresis measured for a powdered sample of  $\text{Li}(\text{MeCN})\text{-}[\text{Er}(\text{tdnCOT})_2]$  at 2 K (average scan rate:  $7 \text{ Oe}\cdot\text{s}^{-1}$ ). The inset shows that the loop is closed at zero field, which was previously observed in related systems and attributed to a magnetic avalanche effect.<sup>29,30</sup>

related to the LF parameters  $A_k^q\langle r^k \rangle$ , as described by eq 4, wherein the Stevens coefficients  $k_{jk}$  are encountered.

$$B_k^q = k_{jk} A_k^q \langle r^k \rangle \quad (4)$$

In order to minimize the number of required parameters, a linear dependence of the values of  $A_k^q\langle r^k \rangle$  on the atomic number was imposed.<sup>16,17,55</sup> In this way, only 6 instead of 15 parameters are required for the five ions  $\text{Tb}^{3+}$ – $\text{Tm}^{3+}$ .

From a given set of LF parameters  $B_k^q$ , the relative energies  $E_i$  of the different wave functions and their Boltzmann occupancies  $p_i$  can be readily obtained. The magnetic susceptibility in the magnetic  $z$  direction can be computed subsequently using the Van Vleck equation (5), with corresponding expressions for the  $x$  and  $y$  directions of the orthogonal system.<sup>56</sup>

$$\chi_z = \frac{\mu_0 \mu_B^2 g_j^2}{kT} \sum_i p_i \left[ \langle \varphi_i | \hat{J}_z | \varphi_i \rangle \langle \varphi_i | \hat{J}_z | \varphi_i \rangle - 2kT \sum_{j \neq i} \frac{\langle \varphi_i | \hat{J}_z | \varphi_j \rangle \langle \varphi_j | \hat{J}_z | \varphi_i \rangle}{E_i - E_j} \right] \quad (5)$$

The values  $p_i$  are the Boltzmann occupancies of the different wave functions  $\varphi_i$ ; the values  $E_i$  represent their relative energies.

Using eq 6, the magnetic susceptibility anisotropies  $\chi_{\text{ax}}$  for the different ions can be obtained, allowing a comparison with experimentally derived values.

$$\chi_{\text{ax}} = \chi_z - \frac{1}{2}(\chi_x + \chi_y) \quad (6)$$

The LF parameter optimization was carried out by minimization of the root-mean-square deviations of these values at different temperatures, using the *Simplex* algorithm.<sup>57</sup> The fitting procedure was implemented in the software *GNU Octave 4.2*<sup>58</sup> (see the SI for the scripts used). In this way, the LF parameters given in Table 2 were obtained, and the splitting of the  $m_j$  sublevels of the individual ions have been computed, as shown in Figure 9.

The energy splitting determined by NMR spectroscopy was then compared with the two sets of values derived from

**Table 2.** LF Parameters ( $\text{cm}^{-1}$ ) for the Individual Ions in  $\text{Ln}(\text{tdnCOT})_2^-$  As Obtained by Fitting of the  $\chi_{\text{ax}}$  Values Determined by Temperature-Dependent  $^2\text{H}$  NMR Measurements

	$\text{Tb}^{3+}$	$\text{Dy}^{3+}$	$\text{Ho}^{3+}$	$\text{Er}^{3+}$	$\text{Tm}^{3+}$
$A_2^0\langle r^2 \rangle$	$-643 \pm 39$	$-571 \pm 62$	$-499 \pm 85$	$-427 \pm 108$	$-355 \pm 131$
$A_4^0\langle r^4 \rangle$	$-651 \pm 26$	$-582 \pm 40$	$-513 \pm 54$	$-444 \pm 68$	$-375 \pm 82$
$A_6^0\langle r^6 \rangle$	$79 \pm 7.1$	$65 \pm 11$	$51 \pm 14$	$37 \pm 17$	$23 \pm 21$

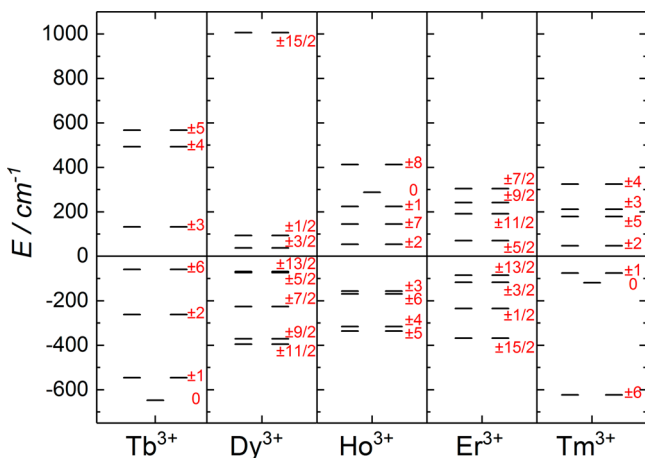


**Figure 9.** Relative energies of the different  $m_j$  sublevels for the individual lanthanide ions in the  $\text{Ln}(\text{tdnCOT})_2^-$  series as obtained from the fitted LF parameters.

computational methods. A comprehensive theoretical study of the entire lanthanide series was reported by Gendron et al.<sup>38</sup> while Ungur et al.<sup>37</sup> only employed calculations for the  $\text{Dy}^{3+}$  and  $\text{Er}^{3+}$  ions. In general, the results from computational studies show a smaller overall LF splitting than those obtained by the method presented herein. Apart from the  $\text{Dy}^{3+}$  ion, the same ground state is found by the computational and our NMR-based approaches. The overall appearance of the energetic splitting of the  $m_j$  manifolds agrees well, as demonstrated for the  $\text{Er}^{3+}$  ion in Figure 10. However, a notable difference occurs

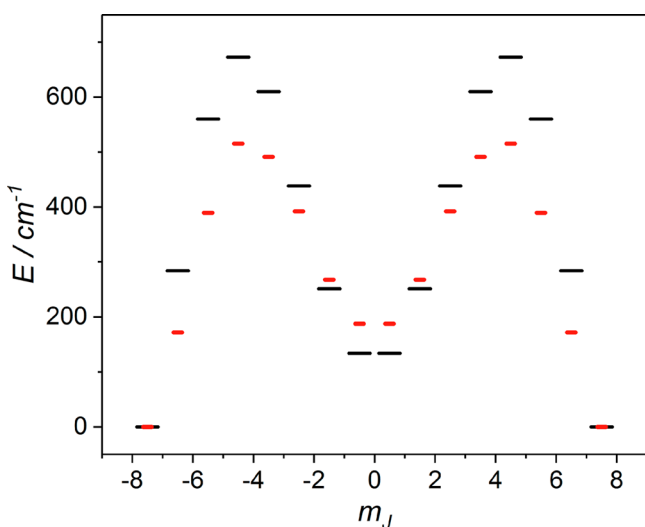


**Figure 10.** Detailed splitting of the  $m_j$  sublevels for the  $\text{Er}^{3+}$  ion in  $\text{Er}(\text{tdnCOT})_2^-$  as obtained from the fitted LF parameters (black) in comparison with values obtained from ab initio calculations (red). Equivalent representations of the remaining  $\text{Ln}^{3+}$  ions are provided in the SI.

for the  $\text{Dy}^{3+}$  ion: the  $m_j = |\pm^{11}/2\rangle$  state is determined as the ground state by our method, while the  $m_j = |\pm^9/2\rangle$  state results from ab initio calculations. This deviation is reflected in the value of  $\chi_{\text{ax}}$  which is negative according to the computations mentioned above but experimentally observed to be positive. In contrast to the computational approach, the  $m_j$  splitting derived by our method explains the sign and magnitude of  $\chi_{\text{ax}}$  for all investigated ions adequately (see Figure S20). Particularly, the irregular temperature dependence of the  $\text{Ho}^{3+}$  ion is reproduced well. At a temperature of ca. 107 K, a zero transition of  $\chi_{\text{ax}}$  is calculated. A similar transition is calculated for  $\text{Dy}^{3+}$  at ca. 437 K (cf. Figure S21).

## SUMMARY

A new series of lanthanide cyclooctatetraene sandwich compounds was synthesized that was used for detailed NMR analysis. A dynamic process leads to two different orientations of the substituents, which both contribute to the average NMR signals in solution. The introduction of  $^2\text{H}$  nuclei permitted the detection of signals over a large temperature range, thus allowing determination of the axial magnetic susceptibility anisotropies  $\chi_{\text{ax}}$  for the five ions  $\text{Tb}^{3+}$ – $\text{Tm}^{3+}$  in the COT sandwich environment.  $\text{Tb}^{3+}$  and  $\text{Ho}^{3+}$  exhibit easy-plane behavior in the investigated temperature range, while  $\text{Dy}^{3+}$ ,  $\text{Er}^{3+}$ , and  $\text{Tm}^{3+}$  are easy-axis systems, in agreement with our previous analysis. The  $\text{Ho}^{3+}$  ion shows a remarkable dependence of  $\chi_{\text{ax}}$  on the temperature, which clearly deviated from  $T^{-2}$ -type behavior. Using the data obtained from the NMR analysis of all synthesized compounds, the LF parameters of the system could be determined. The results of this approach show good agreement with those of ab initio calculations of the system. The electronic structure of the  $\text{Tm}^{3+}$  ion exhibits the required characteristics for a SMM system as well. In particular, the separation between the lowest and first excited-state doublet is very large with approximately  $500 \text{ cm}^{-1}$ .

## EXPERIMENTAL SECTION

**General Procedures.** All reactions were carried out using standard Schlenk or glovebox techniques. Anhydrous solvents were obtained from a MBraun SPS-800 solvent purification system. Anhydrous MeCN was purchased from Sigma-Aldrich, checked for moisture by Karl Fischer titration, and used without further purification. Deuterated THF for NMR spectroscopy was dried by stirring with potassium benzophenone and distilled. Celite was heated for at least 4 h to  $140^\circ\text{C}$  under high vacuum to remove traces of moisture. NMR spectra were recorded on a Bruker AVANCE II NMR spectrometer (9.4 T and 400 MHz for  $^1\text{H}$ ; 61.4 MHz for  $^2\text{H}$ ) or a Bruker AVANCE III NMR spectrometer (14.1 T and 600 MHz for  $^1\text{H}$ ; 92.1 MHz for  $^2\text{H}$ ; 150 MHz for  $^{13}\text{C}$ ). The temperature-controlling unit was calibrated using a standard substance (ethylene glycol in dimethyl sulfoxide or methanol).<sup>59</sup> Spectra were referenced using the residual solvent resonance reported at 1.72 ppm ( $^1\text{H}$  and  $^2\text{H}$ ) and 25.31 ppm ( $^{13}\text{C}$ ).<sup>60</sup> Elemental analyses were carried out at the Microanalytical Laboratory of Heidelberg University using a Vario MICRO cube (Elementar). The ligand tdnCOT was synthesized according to literature methods.<sup>32,39</sup> The partially deuterated equivalent was prepared using the same synthetic route starting from deuterated

xylene (99% D). A detailed description is given in the SI. SQUID measurements were carried out in polycarbonate capsules (Quantum Design, QDS-AGC3). The background measured for one of the capsules was subtracted from the data. A Quantum Design MPMS XL was used for the measurements. The solid material was powdered (agate mortar) before transfer to the capsules. All fitting procedures were carried out using the Solver function of Microsoft Excel 2016, with the exception of the fitting of the LF parameters, which was accomplished using GNU Octave 4.2. Origin 2017 was used for data plotting.

**Synthesis of Li(MeCN)[Ln(tdnCOT)<sub>2</sub>].** The ligand tdnCOT (typically 100 mg, 324 μmol) was dissolved in THF (2 mL). Excess lithium metal band (typically 10 mg) was then added, and the mixture was stirred overnight at ambient temperature. The remaining metal was mechanically removed from the yellow solution and weighed to ensure the consumption of 2 equiv. Anhydrous lanthanide chloride (0.5 equiv) was then added, and the mixture was allowed to stir overnight at ambient temperature. All volatiles were removed under reduced pressure, and the residue was dried under vacuum. Extraction with 10:1 (v/v) toluene/MeCN (2 mL) gave a colored solution and a colorless solid, which were separated by centrifugation. The supernatant was filtered over a short pad of Celite, and all volatiles were removed under reduced pressure to give a colored solid.

**Li(MeCN)[Y(tdnCOT)<sub>2</sub>].** Yield: 51 mg, 68 μmol, 42%.

<sup>1</sup>H NMR (THF-*d*<sub>8</sub>, 295 K, 14.1 T): δ 7.39 (dd, <sup>3</sup>J<sub>H-H</sub> = 5.1 and 3.7 Hz, 8 H, H<sup>5</sup>), 7.16 (dd, <sup>3</sup>J<sub>H-H</sub> = 5.4 and 3.2 Hz, 8 H, H<sup>6</sup>), 5.28 (s, 8 H, H<sup>1</sup>), 3.92 (d, <sup>2</sup>J<sub>H-H</sub> = 14.9 Hz, 8 H, H<sup>3i</sup>), 3.86 (d, <sup>2</sup>J<sub>H-H</sub> = 14.9 Hz, 8 H, H<sup>3o</sup>).

<sup>13</sup>C{<sup>1</sup>H} NMR (THF-*d*<sub>8</sub>, 295 K, 14.1 T): δ 143.4 (s, C<sup>4</sup>), 126.0 (s, C<sup>5</sup>), 125.0 (s, C<sup>6</sup>), 98.9 (d, <sup>1</sup>J<sub>C-Y</sub> = 1.5 Hz, C<sup>2</sup>), 92.5 (d, <sup>1</sup>J<sub>C-Y</sub> = 2.3 Hz, C<sup>1</sup>), 47.3 (s, C<sup>3</sup>).

Elem anal. Calcd: C, 79.68; H, 5.75; N, 1.86. Found: C, 80.14; H, 5.92; N, 1.31.

**Li(MeCN)[Tb(tdnCOT)<sub>2</sub>].** Yield: 134 mg, 163 μmol, 67% (from 150 mg of tdnCOT).

<sup>1</sup>H NMR (THF-*d*<sub>8</sub>, 295 K, 14.1 T): δ 280.3 (s, H<sup>3i</sup>), 116.1 (s, H<sup>1</sup>), 95.3 (s, H<sup>5</sup>), 44.9 (s, H<sup>6</sup>), 29.1 (s, H<sup>3o</sup>).

<sup>13</sup>C{<sup>1</sup>H} NMR (THF-*d*<sub>8</sub>, 295 K, 14.1 T): δ 279.4 (s, C<sup>4</sup>), 244.6 (s, C<sup>3</sup>), 232.5 (s, C<sup>5</sup>), 187.7 (s, C<sup>6</sup>), -597 (s, C<sup>1</sup> or C<sup>2</sup>), -910 (s, C<sup>1</sup> or C<sup>2</sup>).

Elem anal. Calcd: C, 72.90; H, 5.26; N, 1.70. Found: C, 71.75; H, 5.06; N, 0.93.

**Li(MeCN)[Dy(tdnCOT)<sub>2</sub>].** Yield: 114 mg, 137 μmol, 56% (from 150 mg of tdnCOT).

<sup>1</sup>H NMR (THF-*d*<sub>8</sub>, 295 K, 14.1 T): δ 21.6 (s, H<sup>1</sup>), 4.4 (s, H<sup>6</sup>), -0.2 (s, H<sup>3o</sup>), -1.9 (s, H<sup>5</sup>), -28.9 (s, H<sup>3i</sup>).

<sup>13</sup>C{<sup>1</sup>H} NMR (THF-*d*<sub>8</sub>, 295 K, 14.1 T): δ 119.6 (s, C<sup>4</sup>), 116.6 (s, C<sup>5</sup>), 120.1 (s, C<sup>6</sup>), 42.3 (s, C<sup>3</sup>).

Elem anal. Calcd: C, 72.59; H, 5.24; N, 1.69. Found: C, 72.42; H, 5.60; N, 0.99.

**Li(MeCN)<sub>1.5</sub>[Ho(tdnCOT)<sub>2</sub>].** Yield: 82 mg, 96 μmol, 53% (from 113 mg of tdnCOT).

<sup>1</sup>H NMR (THF-*d*<sub>8</sub>, 295 K, 14.1 T): δ 54.5 (s, H<sup>3i</sup>), 20.5 (s, H<sup>5</sup>), 14.3 (s, H<sup>3o</sup>), 13.4 (s, H<sup>6</sup>).

<sup>13</sup>C{<sup>1</sup>H} NMR (THF-*d*<sub>8</sub>, 295 K, 14.1 T): δ 168.1 (s, C<sup>4</sup>), 142.5 (s, C<sup>5</sup>), 135.2 (s, C<sup>6</sup>).

Elem anal. Calcd: C, 72.04; H, 5.28; N, 2.47. Found: C, 72.10; H, 5.45; N, 2.05.

**Li(MeCN)[Er(tdnCOT)<sub>2</sub>].** Yield: 110 mg, 132 μmol, 54% (from 150 mg of tdnCOT).

<sup>1</sup>H NMR (THF-*d*<sub>8</sub>, 295 K, 14.1 T): δ -19.9 (s, H<sup>6</sup>), -41.0 (s, H<sup>3o</sup>), -55.6 (s, H<sup>5</sup>), -76.4 (s, H<sup>1</sup>), -227.6 (s, H<sup>3i</sup>).

<sup>13</sup>C{<sup>1</sup>H} NMR (THF-*d*<sub>8</sub>, 295 K, 14.1 T): δ 80.4 (s, C<sup>6</sup>), 51.3 (s, C<sup>5</sup>), 20.4 (s, C<sup>4</sup>), -82.3 (s, C<sup>3</sup>).

Elem anal. Calcd: C, 72.17; H, 5.21; N, 1.68. Found: C, 71.52; H, 5.44; N, 1.05.

**Li(MeCN)<sub>1.5</sub>[Tm(tdnCOT)<sub>2</sub>].** Yield: 87 mg, 102 μmol, 63%.

<sup>1</sup>H NMR (THF-*d*<sub>8</sub>, 295 K, 14.1 T): δ -35.5 (s, H<sup>6</sup>), -93.2 (s, H<sup>5</sup>).

<sup>13</sup>C{<sup>1</sup>H} NMR (THF-*d*<sub>8</sub>, 295 K, 14.1 T): δ 55.5 (s, C<sup>6</sup>), 6.9 (s, C<sup>5</sup>), -39.3 (s, C<sup>4</sup>).

Elem anal. Calcd: C, 71.70; H, 5.25; N, 2.46. Found: C, 71.01; H, 5.60; N, 2.16.

## ■ ASSOCIATED CONTENT

### 📄 Supporting Information

The Supporting Information is available free of charge on the ACS Publications website at DOI: 10.1021/acs.inorgchem.7b02704.

Synthetic procedures, NMR spectroscopic data at variable temperatures, details of the fitting of the NMR data, DFT-optimized structures, and the script file used for determination of the LF parameters (PDF)

## ■ AUTHOR INFORMATION

### Corresponding Author

\*E-mail: markus.enders@uni-heidelberg.de. Tel: +49-6221-546247. Fax: +49-6221-541616247.

### ORCID

Naoto Ishikawa: 0000-0002-3490-4222

Markus Enders: 0000-0003-0415-1992

### Notes

The authors declare no competing financial interest.

## ■ ACKNOWLEDGMENTS

This work has been supported by the Fonds der Chemischen Industrie with a Kekulé scholarship. The authors acknowledge support by the state of Baden-Württemberg through bwHPC and the German Research Foundation through Grant INST 40/467-1 FUGG. We thank Dr. Marko Damjanović for fruitful discussions and valuable suggestions.

## ■ REFERENCES

- Rinehart, J. D.; Long, J. R. Exploiting single-ion anisotropy in the design of f-element single-molecule magnets. *Chem. Sci.* **2011**, *2* (11), 2078–2085.
- Goodwin, C. A. P.; Ortu, F.; Reta, D.; Chilton, N. F.; Mills, D. P. Molecular magnetic hysteresis at 60 K in dysprosocenium. *Nature* **2017**, *548* (7668), 439–442.
- Guo, F. S.; Day, B. M.; Chen, Y. C.; Tong, M. L.; Mansikkamaki, A.; Layfield, R. A. A Dysprosium Metallocene Single-Molecule Magnet Functioning at the Axial Limit. *Angew. Chem., Int. Ed.* **2017**, *56* (38), 11445–11449.
- Ding, Y.-S.; Chilton, N. F.; Winpenny, R. E. P.; Zheng, Y.-Z. On Approaching the Limit of Molecular Magnetic Anisotropy: A Near-Perfect Pentagonal Bipyramidal Dysprosium(III) Single-Molecule Magnet. *Angew. Chem., Int. Ed.* **2016**, *55* (52), 16071–16074.
- Rinehart, J. D.; Fang, M.; Evans, W. J.; Long, J. R. A N<sub>2</sub><sup>3-</sup> Radical-Bridged Terbium Complex Exhibiting Magnetic Hysteresis at 14 K. *J. Am. Chem. Soc.* **2011**, *133* (36), 14236–14239.
- Ungur, L.; Chibotaru, L. F. Strategies toward High-Temperature Lanthanide-Based Single-Molecule Magnets. *Inorg. Chem.* **2016**, *55* (20), 10043–10056.
- Liddle, S. T.; van Slageren, J. Improving f-element single molecule magnets. *Chem. Soc. Rev.* **2015**, *44* (19), 6655–6669.
- McAdams, S. G.; Ariciu, A.-M.; Kostopoulos, A. K.; Walsh, J. P. S.; Tuna, F. Molecular single-ion magnets based on lanthanides and actinides: Design considerations and new advances in the context of quantum technologies. *Coord. Chem. Rev.* **2017**, *346*, 216–239.
- Ungur, L.; Chibotaru, L. F. Ab Initio Crystal Field for Lanthanides. *Chem. - Eur. J.* **2017**, *23* (15), 3708–3718.
- Rechkemmer, Y.; Fischer, J. E.; Marx, R.; Dörfel, M.; Neugebauer, P.; Horvath, S.; Gysler, M.; Brock-Nannestad, T.; Frey, W.; Reid, M. F.; van Slageren, J. Comprehensive Spectroscopic

Determination of the Crystal Field Splitting in an Erbium Single-Ion Magnet. *J. Am. Chem. Soc.* **2015**, *137* (40), 13114–13120.

(11) Görller-Walrand, C.; Binneemans, K. In *Handbook on the Physics and Chemistry of Rare Earths*; Gschneidner, K. A., Eyring, L., Eds.; North Holland, 1996; Chapter 155, Vol. 23, pp 121–283.

(12) Flanagan, B. M.; Bernhardt, P. V.; Krausz, E. R.; Lüthi, S. R.; Riley, M. J. Ligand-Field Analysis of an Er(III) Complex with a Heptadentate Tripodal  $N_4O_3$  Ligand. *Inorg. Chem.* **2001**, *40* (21), 5401–5407.

(13) Flanagan, B. M.; Bernhardt, P. V.; Krausz, E. R.; Lüthi, S. R.; Riley, M. J. A Ligand-Field Analysis of the trensal ( $H_3trensal = 2,2',2''$ -Tris(salicylideneimino)triethylamine) Ligand. An Application of the Angular Overlap Model to Lanthanides. *Inorg. Chem.* **2002**, *41* (20), 5024–5033.

(14) Cucinotta, G.; Perfetti, M.; Luzon, J.; Etienne, M.; Car, P.-E.; Caneschi, A.; Calvez, G.; Bernot, K.; Sessoli, R. Magnetic Anisotropy in a Dysprosium/DOTA Single-Molecule Magnet: Beyond Simple Magneto-Structural Correlations. *Angew. Chem., Int. Ed.* **2012**, *51* (7), 1606–1610.

(15) Perfetti, M.; Lucaccini, E.; Sorace, L.; Costes, J. P.; Sessoli, R. Determination of magnetic anisotropy in the LnTRENALS complexes (Ln = Tb, Dy, Er) by torque magnetometry. *Inorg. Chem.* **2015**, *54* (7), 3090–3092.

(16) Ishikawa, N.; Iino, T.; Kaizu, Y. Determination of Ligand-Field Parameters and f-Electronic Structures of Hetero-Dinuclear Phthalocyanine Complexes with a Diamagnetic Yttrium(III) and a Paramagnetic Trivalent Lanthanide Ion. *J. Phys. Chem. A* **2002**, *106* (41), 9543–9550.

(17) Ishikawa, N.; Sugita, M.; Okubo, T.; Tanaka, N.; Iino, T.; Kaizu, Y. Determination of Ligand-Field Parameters and f-Electronic Structures of Double-Decker Bis(phthalocyaninato)lanthanide Complexes. *Inorg. Chem.* **2003**, *42* (7), 2440–2446.

(18) Ishikawa, N.; Sugita, M.; Ishikawa, T.; Koshihara, S.-y.; Kaizu, Y. Lanthanide Double-Decker Complexes Functioning as Magnets at the Single-Molecular Level. *J. Am. Chem. Soc.* **2003**, *125* (29), 8694–8695.

(19) Novikov, V. V.; Pavlov, A. A.; Belov, A. S.; Vologzhanina, A. V.; Savitsky, A.; Voloshin, Y. Z. Transition Ion Strikes Back: Large Magnetic Susceptibility Anisotropy in Cobalt(II) Clathrochelates. *J. Phys. Chem. Lett.* **2014**, *5* (21), 3799–3803.

(20) Novikov, V. V.; Pavlov, A. A.; Nelyubina, Y. V.; Boulon, M.-E.; Varzatskii, O. A.; Voloshin, Y. Z.; Winpenny, R. E. P. A Trigonal Prismatic Mononuclear Cobalt(II) Complex Showing Single-Molecule Magnet Behavior. *J. Am. Chem. Soc.* **2015**, *137* (31), 9792–9795.

(21) Damjanovic, M.; Katoh, K.; Yamashita, M.; Enders, M. Combined NMR Analysis of Huge Residual Dipolar Couplings and Pseudocontact Shifts in Terbium(III)-Phthalocyaninato Single Molecule Magnets. *J. Am. Chem. Soc.* **2013**, *135* (38), 14349–14358.

(22) Damjanovic, M.; Morita, T.; Katoh, K.; Yamashita, M.; Enders, M. Ligand pi-radical interaction with f-shell unpaired electrons in phthalocyaninato-lanthanoid single-molecule magnets: a solution NMR spectroscopic and DFT study. *Chem. - Eur. J.* **2015**, *21* (41), 14421–14432.

(23) Damjanović, M.; Morita, T.; Horii, Y.; Katoh, K.; Yamashita, M.; Enders, M. How Ions Arrange in Solution: Detailed Insight from NMR Spectroscopy of Paramagnetic Ion Pairs. *ChemPhysChem* **2016**, *17* (21), 3423–3429.

(24) Damjanovic, M.; Samuel, P. P.; Roesky, H. W.; Enders, M. NMR analysis of an Fe(I)-carbene complex with strong magnetic anisotropy. *Dalton Trans* **2017**, *46* (16), 5159–5169.

(25) Hiller, M.; Maier, M.; Wadepohl, H.; Enders, M. Paramagnetic NMR Analysis of Substituted Biscyclooctatetraene Lanthanide Complexes. *Organometallics* **2016**, *35* (11), 1916–1922.

(26) Suturina, E. A.; Mason, K.; Geraldes, C. F. G. C.; Kuprov, I.; Parker, D. Beyond Bleaney's Theory: Experimental and Theoretical Analysis of Periodic Trends in Lanthanide-Induced Chemical Shift. *Angew. Chem., Int. Ed.* **2017**, *56* (40), 12215–12218.

(27) Jeletic, M.; Lin, P.-H.; Le Roy, J. J.; Korobkov, I.; Gorelsky, S. I.; Murugesu, M. An Organometallic Sandwich Lanthanide Single-Ion

Magnet with an Unusual Multiple Relaxation Mechanism. *J. Am. Chem. Soc.* **2011**, *133* (48), 19286–19289.

(28) Le Roy, J. J.; Jeletic, M.; Gorelsky, S. I.; Korobkov, I.; Ungur, L.; Chibotaru, L. F.; Murugesu, M. An Organometallic Building Block Approach To Produce a Multidecker 4f Single-Molecule Magnet. *J. Am. Chem. Soc.* **2013**, *135* (9), 3502–3510.

(29) Meihaus, K. R.; Long, J. R. Magnetic blocking at 10 K and a dipolar-mediated avalanche in salts of the bis(eta<sup>8</sup>-cyclooctatetraenide) complex [Er(COT)<sub>2</sub>]. *J. Am. Chem. Soc.* **2013**, *135* (47), 17952–17957.

(30) Le Roy, J. J.; Korobkov, I.; Murugesu, M. A sandwich complex with axial symmetry for harnessing the anisotropy in a prolate erbium(III) ion. *Chem. Commun.* **2014**, *50* (13), 1602–1604.

(31) Vonci, M.; Mason, K.; Suturina, E. A.; Frawley, A. T.; Worswick, S. G.; Kuprov, I.; Parker, D.; McInnes, E. J. L.; Chilton, N. F. Rationalization of Anomalous Pseudocontact Shifts and Their Solvent Dependence in a Series of C<sub>3</sub>-Symmetric Lanthanide Complexes. *J. Am. Chem. Soc.* **2017**, *139* (40), 14166–14172.

(32) Wender, P. A.; Christy, J. P. Nickel(0)-Catalyzed [2 + 2 + 2 + 2] Cycloadditions of Terminal Dienes for the Synthesis of Substituted Cyclooctatetraenes. *J. Am. Chem. Soc.* **2007**, *129* (44), 13402–13403.

(33) Bleaney, B. Nuclear magnetic resonance shifts in solution due to lanthanide ions. *J. Magn. Reson.* **1972**, *8* (1), 91–100.

(34) Funk, A. M.; Finney, K.-L. N. A.; Harvey, P.; Kenwright, A. M.; Neil, E. R.; Rogers, N. J.; Kanthi Senanayake, P.; Parker, D. Critical analysis of the limitations of Bleaney's theory of magnetic anisotropy in paramagnetic lanthanide coordination complexes. *Chem. Sci.* **2015**, *6* (3), 1655–1662.

(35) Blackburn, O. A.; Edkins, R. M.; Faulkner, S.; Kenwright, A. M.; Parker, D.; Rogers, N. J.; Shuvaev, S. Electromagnetic susceptibility anisotropy and its importance for paramagnetic NMR and optical spectroscopy in lanthanide coordination chemistry. *Dalton Trans* **2016**, *45* (16), 6782–6800.

(36) Sievers, J. Asphericity of 4f-shells in their Hund's Rule Ground State. *Z. Phys. B: Condens. Matter Quanta* **1982**, *45*, 289–296.

(37) Ungur, L.; Le Roy, J. J.; Korobkov, I.; Murugesu, M.; Chibotaru, L. F. Fine-tuning the local symmetry to attain record blocking temperature and magnetic remanence in a single-ion magnet. *Angew. Chem., Int. Ed.* **2014**, *53* (17), 4413–4417.

(38) Gendron, F.; Pritchard, B.; Bolvin, H.; Autschbach, J. Single-ion 4f element magnetism: an ab-initio look at Ln(COT)<sub>2</sub><sup>-</sup>. *Dalton Trans.* **2015**, *44* (46), 19886–19900.

(39) Wender, P. A.; Lesser, A. B.; Sirois, L. E. Rhodium dinaphthocyclooctatetraene complexes: synthesis, characterization and catalytic activity in [5 + 2] cycloadditions. *Angew. Chem., Int. Ed.* **2012**, *51* (11), 2736–2740.

(40) Bertini, I.; Luchinat, C. Relaxation. *Coord. Chem. Rev.* **1996**, *150*, 77–110.

(41) Bertini, I.; Luchinat, C.; Parigi, G. *Solution NMR of Paramagnetic Molecules—Applications to Metallobiomolecules and Models*; Elsevier, 2001; Vol. 2.

(42) Bothner-By, A. A. *eMagRes*; John Wiley & Sons, Ltd., 2007; pp 2932–2938.

(43) Reilley, C. N.; Good, B. W.; Allendoerfer, R. D. Separation of contact and dipolar lanthanide induced nuclear magnetic resonance shifts: evaluation and application of some structure independent methods. *Anal. Chem.* **1976**, *48* (11), 1446–1458.

(44) Reuben, J. Structural information from chemical shifts in lanthanide complexes. *J. Magn. Reson.* **1982**, *50* (2), 233–236.

(45) Pinkerton, A. A.; Rossier, M.; Spiliadis, S. Lanthanide-induced contact shifts. the average electron spin polarization, theory and experiment. *J. Magn. Reson.* **1985**, *64* (3), 420–425.

(46) Peters, J. A.; Huskens, J.; Raber, D. J. Lanthanide induced shifts and relaxation rate enhancements. *Prog. Nucl. Magn. Reson. Spectrosc.* **1996**, *28* (3–4), 283–350.

(47) Knorr, R.; Hauer, H.; Weiss, A.; Polzer, H.; Ruf, F.; Löw, P.; Dvortsák, P.; Böhrer, P. Unpaired Spin Densities from NMR Shifts<sup>†</sup> and Magnetic Anisotropies of Pseudotetrahedral Cobalt(II) and

Nickel(II) Vinamidine Bis(chelates)<sup>†</sup>. *Inorg. Chem.* **2007**, *46* (20), 8379–8390.

(48) Domaille, P. J.; Harlow, R. L.; Ittel, S. D.; Peet, W. G. NMR spectra of paramagnetic Group VIII complexes of bis(pyridylimino)-isindoline. *Inorg. Chem.* **1983**, *22* (26), 3944–3952.

(49) Bastiaan, E. W.; Maclean, C.; Van Zijl, P. C. M.; Bothner, A. A. High-Resolution NMR of Liquids and Gases: Effects of Magnetic-Field-Induced Molecular Alignment. *Annu. Rep. NMR Spectrosc.* **1987**, *19*, 35–77.

(50) Mantsch, H. H.; Saitô, H.; Smith, I. C. P. Deuterium magnetic resonance, applications in chemistry, physics and biology. *Prog. Nucl. Magn. Reson. Spectrosc.* **1977**, *11* (4), 211–272.

(51) Bothner-By, A. A.; Gayathri, C.; Van Zijl, P. C. M.; MacLean, C. Anisotropy of the diamagnetic susceptibility of benzene. Determination by high-field deuterium NMR. *J. Magn. Reson.* **1984**, *56* (3), 456–462.

(52) Harriman, K. L.; Murugesu, M. An Organolanthanide Building Block Approach to Single-Molecule Magnets. *Acc. Chem. Res.* **2016**, *49* (6), 1158–1167.

(53) Harriman, K. L. M.; Korobkov, I.; Murugesu, M. From a Piano Stool to a Sandwich: A Stepwise Route for Improving the Slow Magnetic Relaxation Properties of Thulium. *Organometallics* **2017**, DOI: [10.1021/acs.organomet.7b00449](https://doi.org/10.1021/acs.organomet.7b00449).

(54) Abragam, A.; Bleaney, B. *Electron Paramagnetic Resonance of Transition Ions*; Oxford University Press, 1970.

(55) Ishikawa, N. Simultaneous Determination of Ligand-Field Parameters of Isostructural Lanthanide Complexes by Multidimensional Optimization. *J. Phys. Chem. A* **2003**, *107* (30), 5831–5835.

(56) Van Vleck, J. H. *The Theory of Electric and Magnetic Susceptibilities*; Oxford University Press, 1932.

(57) Nelder, J. A.; Mead, R. A Simplex Method for Function Minimization. *Computer Journal* **1965**, *7* (4), 308–313.

(58) Eaton, J. W.; Bateman, D.; Hauberg, S.; Wehbring, R. *GNU Octave version 3.8.1 manual: a high-level interactive language for numerical computations*; CreateSpace Independent Publishing Platform, 2014.

(59) Findeisen, M.; Brand, T.; Berger, S. A <sup>1</sup>H-NMR thermometer suitable for cryoprobes. *Magn. Reson. Chem.* **2007**, *45* (2), 175–178.

(60) Fulmer, G. R.; Miller, A. J. M.; Sherden, N. H.; Gottlieb, H. E.; Nudelman, A.; Stoltz, B. M.; Bercaw, J. E.; Goldberg, K. I. NMR Chemical Shifts of Trace Impurities: Common Laboratory Solvents, Organics, and Gases in Deuterated Solvents Relevant to the Organometallic Chemist. *Organometallics* **2010**, *29* (9), 2176–2179.